Inorganic Chemistry

Article

pubs.acs.org/IC

Magnetodielectric Effect in Crystals of the Noncentrosymmetric CaOFeS at Low Temperature

Charlène Delacotte,[†] Olivier Pérez,[†] Alain Pautrat,[†] David Berthebaud,[†] Sylvie Hébert,[†] Emmanuelle Suard,[‡] Denis Pelloquin,*[,†] and Antoine Maignan[†]

[†]Laboratoire CRISMAT ENSICAEN, UMR CNRS 6508, 6 Boulevard du Maréchal Juin, 14050 Caen Cedex 04, France

[‡]Institut Laue-Langevin (ILL), 71 avenue des Martyrs, 38042 Grenoble Cedex 9, France

Supporting Information

ABSTRACT: Single crystals of the stoichiometric iron calcium oxysulfide CaOFeS have been grown by a solid-state reaction. Structural analysis of CaOFeS at room temperature by combining single-crystal X-ray diffraction data and transmission electron microscopy leads to a stoichiometric hexagonal noncentrosymmetric $P6_3mc$ layered structure isostructural to CaOZnS. It is built from alternating layers made of $FeOS_3$ tetrahedra sharing sulfur apexes and stacked with Ca^{2+} planes. All Fe−O bonds are parallel to the stacking axis; this breaks the centrosymmetry, leading to a polar structure. The dielectric measurements reveal the existence of a magnetodielectric effect near 33 K in good agreement with the Neel temperature, as evidenced near 35 K by specific heat measurements reported by a different group.

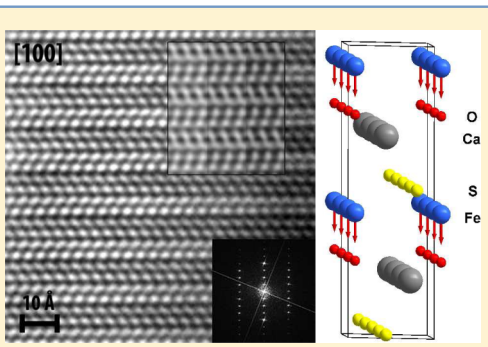

INTRODUCTION

Transition-metal oxides exhibit such a wide range of physical and chemical properties that they find applications in numerous sectors such as heterogeneous catalysis, magnetic recording compounds, batteries, solid oxide fuel cells, etc. In parallel to the search for new phases, a lot of attention has been devoted to metal/ion substitutions to improve the properties of oxides or to induce new ones. Especially, a peculiar attention has been given to control of these properties, taking advantage of the anion framework. Some recent and promising results have been reported in the area of mixed-anion chemistry such as, for instance, some superconductivity or optical properties in oxychalcogenides or oxypnictides (for instance, reviews by Clarke et al.[1] and Johrendt et al.[2] and references cited therein).

Considering the existence of several layered Ae−M−O−Ch phases (Ae = alkaline earth; M = Mn, Fe, Co, Cu, Zn; Ch = S, Se), the introduction of sulfur was also considered in the Ca−Fe−O system. The synthesis of the iron sulfide CaOFeS was first reported more than 20 years,[3,4] but its structural and physical properties were recently investigated on powder data.[5]

In the present study, we report on the structure and electric properties of CaOFeS single crystals prepared by a solid-state reaction. The structure has been established at room temperature by combining data from transmission electron microscopy (TEM) observations [electron diffraction (ED) and high-resolution electron microscopy (HREM)] together with single-crystal X-ray diffraction data. The Rietveld refinements jointly performed on corresponding neutron powder diffraction (NPD) data point also toward a stoichiometric CaOFeS composition that is isostructural to that of the CaOZnS polar structure.[6,7] The CaOFeS compound exhibits a semiconducting behavior and, in addition, the thermal dependence of the dielectric permittivity has been measured at low temperature.

EXPERIMENTAL SECTION

Syntheses. Iron calcium oxysulfide (CaOFeS) powder and single crystals were synthesized by a standard solid-state reaction process using CaO (stored at 900 °C prior to use), iron, and sulfur as the starting materials in a 1:1:1 ratio. The powders were mixed, ground, and uniaxially pressed at about 3 tons/cm^2 into bars (10 × 2 × 2 mm^3). Then, the bars were put into an alumina crucible and sealed under vacuum in a silica tube. The ampule was heated for 12 h at 950 °C in a tubular furnace. Platelet-like single crystals have also been grown from the same precursors but using a thermal process in two steps: heating for first 6 h at 500 °C and then 12 h at 950 °C with a controlled cooling in 6 h down to room temperature.

Diffraction Data. The powder X-ray diffraction (PXRD) data were collected using an XpertPro Panalytical diffractometer working with Co Kα radiation and equipped with an X'Celerator detector. Collection was made over an angular range of $5° \leq 2\theta \leq 120°$. NPD data were collected at room temperature on a D2B diffractometer at the ILL reactor using wavelength λ = 1.594 Å. The sample was put into a cylindrical vanadium can. Single-crystal X-ray diffraction measurements were performed using Mo Kα radiation produced with a microfocus Incoatec Iμs sealed X-ray tube on a Kappa charge-coupled-device (CCD; Bruker-Nonius) four-circle diffractometer equipped with a bidimensional detector. A single crystal (SC), with approximate dimensions of 0.33 mm × 0.43 mm × 0.016 mm, was used for X-ray crystallographic analysis. The data collection consists of large ω and φ scans of the reciprocal space; a total of 3302 frames were collected with an exposure time of 5−15°/frame depending of the θ value.

Received: April 17, 2015
Published: June 18, 2015

DOI: 10.1021/acs.inorgchem.5b00879
Inorg. Chem. 2015, 54, 6560−6565

Electron Microscopy. Lattice constants and space groups were deduced from the ED study carried out with a JEOL 2010CX transmission electron microscope tilting around crystallographic axes. HREM was performed with a TECNAI G^2 UT microscope operating at 300 kV (point resolution 1.7 Å; C_S = 0.7 mm). Both microscopes were equipped with energy-dispersive spectroscopy (EDS) analyzers. The simulated HREM images were calculated with *JEMS* software. Scanning electron microscopy (SEM) images were recorded with a Zeiss field-emission gun microscope operating at 20 kV and equipped with an EDAX analyzer.

Physical Properties. The transport properties (four-probe method) were investigated by means of a physical property measurement system (PPMS), while susceptibility and magnetization were measured from a direct-current SQUID Quantum Design magnetometer. Dielectric measurements were also performed on single crystals using a homemade probe in a PPMS 14 T. Silver electrodes were painted on the parallel largest faces of the single crystal of regular shape (0.25 mm^2), and copper leads were fixed to these electrodes. Then, the contacts were dried in an oven at 100 °C. The capacitance and dissipation factor were measured as a function of the temperature and frequency with an Agilent 4284A LCR meter.

RESULTS AND DISCUSSION

Structural Part. According to the experimental process described above, the powder of CaOFeS was analyzed by PXRD data collected at room temperature. Its pattern evidenced the formation of the expected CaOFeS phase as the main phase.[4,5] Nevertheless, some unidentified extra peaks were found. In order to check the purity, this sample was studied by TEM techniques. The room temperature ED tilting along the larger cell parameter (Figure 1) allowed for building of the reciprocal space. The latter reveal a hexagonal unit cell ($a \approx 3.8$ Å; $c \approx 11.4$ Å) as the main phase with the observed existence conditions hkl: $l = 2n$ and $00l$: $l = 2n$. Note that, on the [010] ED pattern, double diffraction is observed along the c^* axis. Taking into account these extinction conditions, three space groups can be proposed: $P6_3mc$, $P\bar{6}2c$, or $P6_3/mmc$. In addition, this work allowed identification of an unknown phase crystallizing in an orthorhombic C-type cell (11.1 × 11.2 × 17.5 $Å^3$). EDS analyses coupled to this ED study reinforce our preliminary phase analysis based on the PXRD pattern by giving the average 1:1:1 content of Fe/Ca/S ions for the main phase (with O being too light to be analyzed). Fe/Ca ∼ 1.25 and Fe/S ∼ 1 ratios are observed for the secondary unknown phase detected in the as-prepared powder sample. All of our attempts to avoid the formation of this secondary phase failed. So, fine structural analysis was on single crystals performed. Analysis of their X-ray diffraction data also allowed us to judge the actual symmetry. The experimental frames, showing the good crystalline quality of the samples, led to the following cell parameters: $a \approx b \approx 3.75$ Å, $c \approx 11.35$ Å, $\alpha \approx \beta \approx 90°$, and $\gamma \approx 120°$, in agreement with the first ED analyses on the bulk CaOFeS phase. Corresponding EDS measurements on selected single crystals confirmed this chemical composition. Nevertheless, some additional SEM images recorded on these selected single crystals revealed the systematic presence of a kind of surface coating all around the single crystal (cross section in Figure 2). That layer is very weak (thickness ≈ 0.3 μm), and the corresponding EDS analyses at the level of that coating did not evidence significant chemical deviation compared to the expected one. However, that coating clearly exhibits a chemical contrast in the Figure 2b image in comparison with the crystal core. So, that amorphous skin could be induced by a partial reactivity in air of the as-grown crystals. Plots of reciprocal lattice planes were assembled from

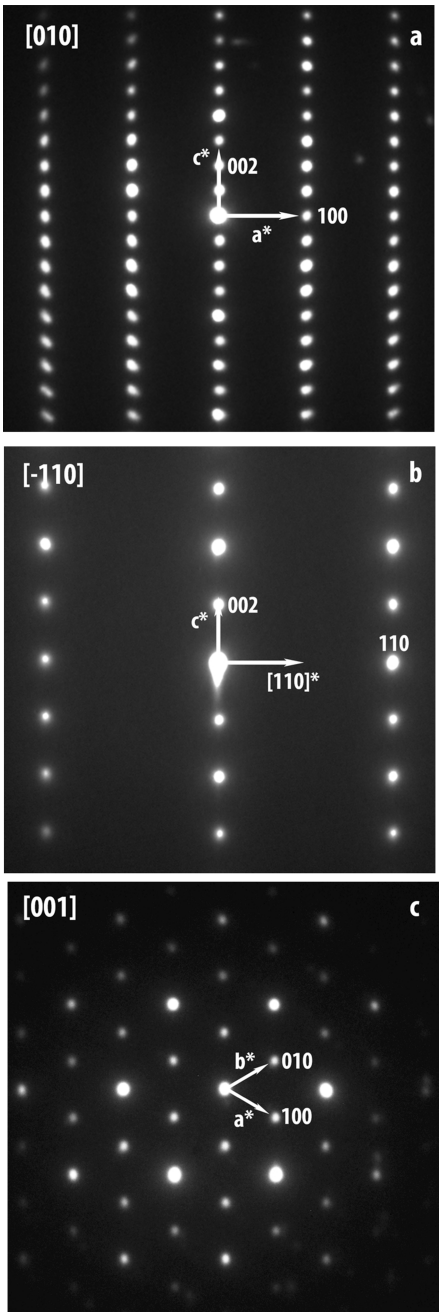

Figure 1. ED patterns of (a) [010], (b) [−110], and (c) [001] zone axes.

the different scans; they provide an overall view of the reciprocal space. The conditions limiting the possible reflections are hhl: $l = 2n$, $00l$: $l = 2n$ in agreement with the $P6_3mc$, $P\bar{6}2c$, and $P6_3/mmc$ space groups. The frames were integrated with the Bruker *SAINT* software package using a narrow-frame algorithm. The integration of the data using a hexagonal unit cell yielded a total of 8978 reflections to a maximum θ angle of 52.20° (0.45 Å resolution). The final cell constants of $a = 3.7519(9)$ Å, $c = 11.349(3)$ Å, and volume = 138.35(9) $Å^3$ are based upon the refinement of the XYZ centroids of 6746 reflections above 20 $\sigma(I)$ with 10.78° < 2θ < 105.0°. Data were corrected from absorption using the *SADABS* program[8] developed for scaling and absorption corrections of the area detector data; the ratio of minimum to maximum apparent transmission was 0.136; Bijvoet's

DOI: 10.1021/acs.inorgchem.5b00879
Inorg. Chem. 2015, 54, 6560−6565

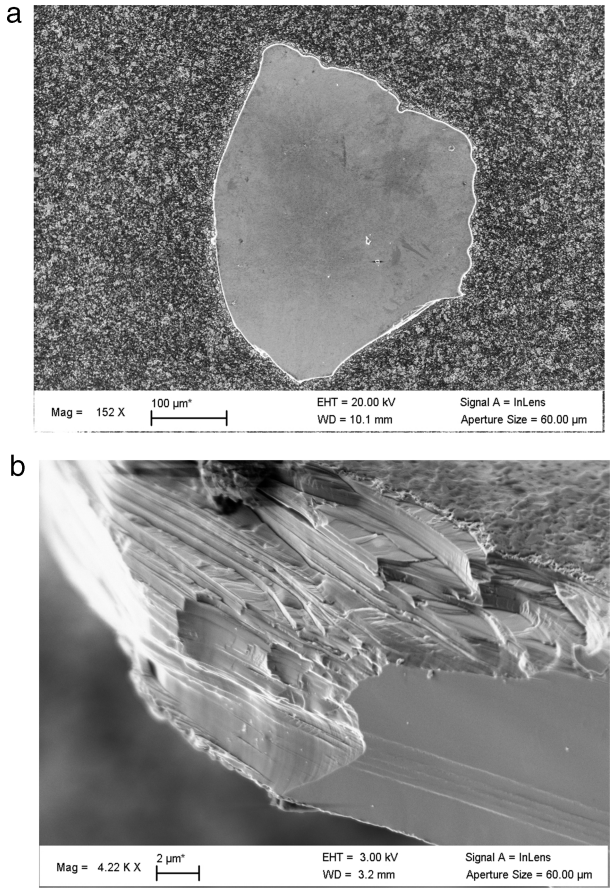

Figure 2. SEM images of a single crystal (a) surface and (b) cross section.

reflection pairs were not merged. A Wilson plot, which provides a good figure of merit with regard to the centricity/acentricity, leads to a $\langle |E^2 - 1| \rangle$ value, in agreement with a noncentrosymmetric structure. Moreover, a space group determination has been performed using a charge-flipping algorithm[9] with *Superflip* software.[10,11] From a structure solution in the space group *P*1, the electron density can be interpreted in terms of the symmetry element. This symmetry analysis leads to a list of all the symmetry operations compatible with the lattice. On the basis of the agreement factor assigned to each symmetry operation, the space group is $P6_3mc$; the *m* mirror perpendicular to *c* is not compatible with the electron density. Following all of these different analyses, the noncentrosymmetric space group $P6_3mc$ was chosen. The structure was then determined with *Superflip*, and the corresponding model was introduced in the program *Jana2006*.[12] This first model is constituted of one Fe, one Ca, one S, and one O sites. All of the atomic positions were refined, and then anisotropic displacement parameters (ADPs) were considered for all of the atoms. At this step, one inversion center was introduced as twin law, and a twin fraction was refined (Flack parameter[13]); the result was in agreement with an enantiopure crystal. The final agreement factor was equal to 0.026 for a goodness of fit of 1.5. Atomic parameters and distances for the sample are summarized in Tables 1 and 2 respectively (see the Supporting Information, SI).

Table 2. Interatomic Distances of CaOFeS According to SC and NPD Refinements

atom−atom	*d* (Å) NPD	*d* (Å) SC
Ca−O (3×)	2.298(4)	2.301(5)
Ca−S (3×)	2.982(9)	2.969(4)
Fe−S (3×)	2.391(6)	2.386(2)
Fe−O (1×)	1.88(1)	1.87(2)

In parallel to this single-crystal investigation, NPD data collected at room temperature have also been refined considering the structural model deduced from our single-crystal analysis (see the SI). Atomic positions and distances refined from NPD analyses are also summarized in Tables 1 and 2, respectively. A good agreement is observed both with the results deduced from our single-crystal refinements and with the previous structural determination.[5] These results point out definitively a stoichiometric CaOFeS structure.

The structure can be described as a layered structure along the [001] direction with succession of top-shared $FeOS_3$ tetrahedral layers spaced by calcium rows (Figure 3a). Each $FeOS_3$ tetrahedron is built from three S atoms in the *ab* plane and one apical O (Figure 3b) and shares all of its S anions with two other $FeOS_3$ to form a triangular iron network (Figure 3c). Ca atoms are surrounded by three S atoms 2.97 Å away and three O atoms 2.30 Å away, which form edge-shared octahedral blocks. All $FeOS_3$ tetrahedra are oriented along the stacking axis, leading to a dipole moment directed along the Fe−O

Table 1. Atomic Parameters from Single-Crystal (SC) and NPD Refinements

						z			
atom	oxidation state	Wyckoff	occ.	*x*	*y*	SC	NPD	SC u_{eq} (Å^2)	NPD u_{iso} (Å^2)
Fe	2+	2a	1	0	0	0.4402(2)	0.4410(4)	0.0115(5)	0.011(1)
Ca	2+	2b	1	$^1/_3$	$^2/_3$	0.7071(3)	0.7092(9)	0.0091(5)	0.006(2)
S	2−	2b	1	$^2/_3$	$^1/_3$	0.5282(3)	0.529(1)	0.0094(9)	0.010(4)
O	2−	2a	1	0	0	0.276(1)	0.2759(5)	0.009(2)	0.010(2)

NPD refinement report: $a = b = 3.75846(6)$ Å, $c = 11.3722(3)$ Å, space group $P6_3mc$, $R_{Bragg} = 4.62\%$, $R_{wp} = 3.78\%$

SC refinement report: $a = b = 3.7519(9)$ Å, $c = 11.349(3)$ Å, space group $P6_3mc$, $R_{obs} = 2.58\%$, GOF(obs) = 1.50, indep refIns with $I \geq 3\sigma(I) = 635$

ADP Harmonic Parameters

atom	u_{11} (Å^2)	u_{22} (Å^2)	u_{33} (Å^2)	u_{12} (Å^2)
Fe	0.0137(6)	0.0137(6)	0.0072(9)	0.0068(3)
Ca	0.0071(6)	0.0071(6)	0.0131(9)	0.0036(3)
S	0.008(1)	0.008(1)	0.012(2)	0.0041(5)
O	0.010(2)	0.010(2)	0.007(5)	0.005(1)

DOI: 10.1021/acs.inorgchem.5b00879
Inorg. Chem. 2015, 54, 6560−6565

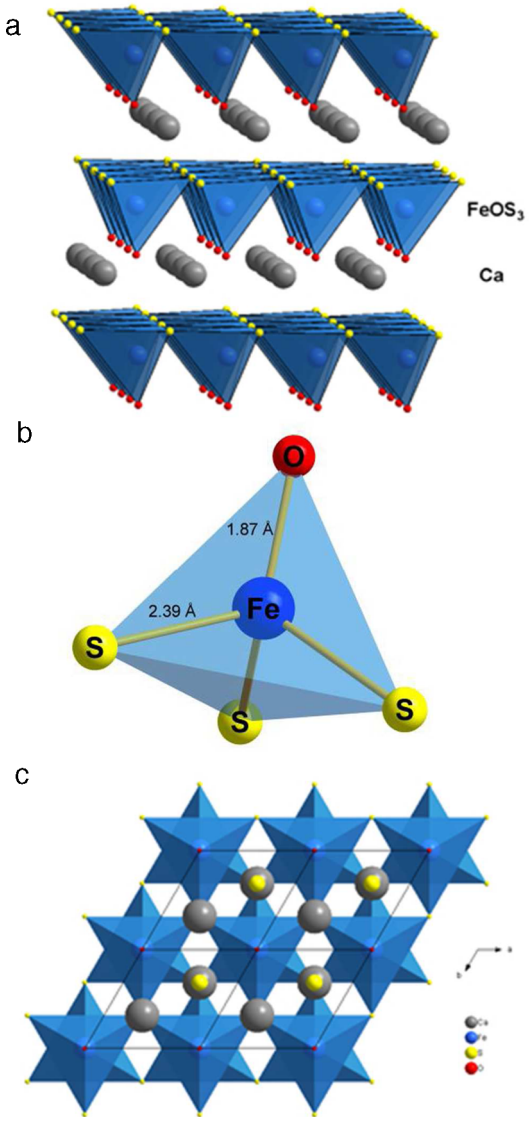

Figure 3. Crystal structure of CaOFeS along the (a) [100] and (c) [001] directions. A detailed $FeOS_3$ tetrahedron is shown in part b.

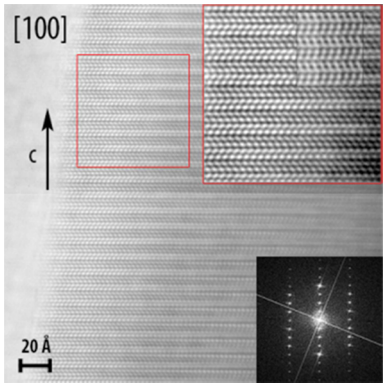

Figure 4. [100] HREM image and corresponding fast Fourier transform pattern of CaOFeS collected with a defocus value close to −80 nm. The simulated image with a thickness ranging from 2 to 5 nm is presented in the right part of the inset.

bond. Clearly, CaOFeS is isostructural with the polar CaOZnS compound.[6,7] To complete this structural analysis and evaluate the homogeneity of the stacking mode, a HREM study was also

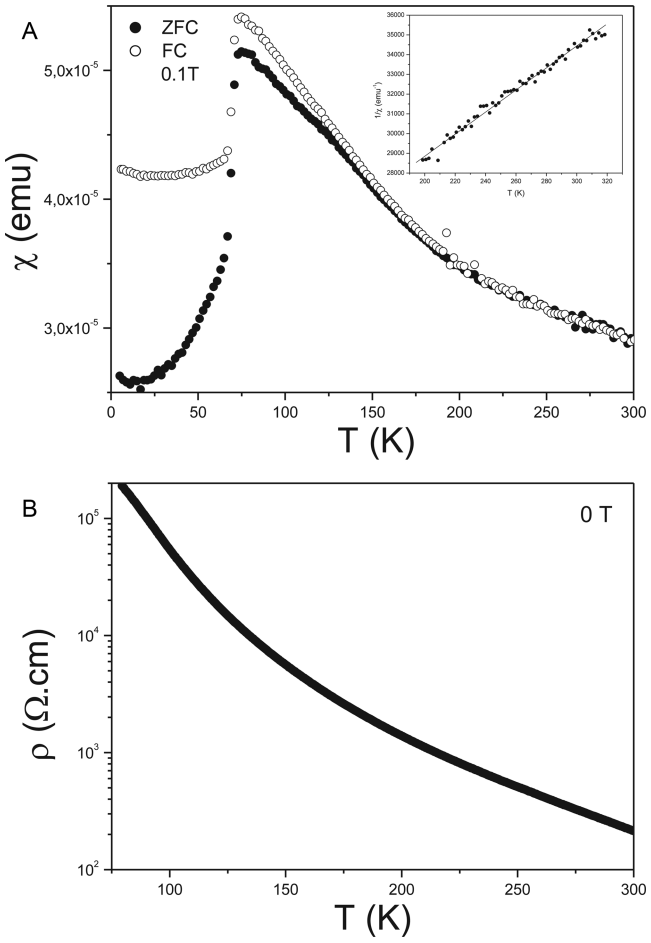

Figure 5. Thermal dependence of the (a) magnetic susceptibility and (b) electrical resistivity carried out on a single crystal.

performed. No intergrowth defects or local ordering phenomena have been detected, as illustrated in Figure 4. Note that simulated images fit well with the experimental ones, as illustrated by the [100]-oriented HREM enlargement image shown in the inset in Figure 4.

Although CaOFeS is characterized by a polar noncentrosymmetric space group and thus exhibits a symmetry that may lead to ferroelectricity, its crystal structure precludes such behavior. To be ferroelectric, the dipole moment (directed along the Fe−O bond) must be able to switch by reversal of the applied electric field (bipolar switching), which is not permitted by the network of the stacked tetrahedra. However, the known polarity of the compound presents sufficient interest for dielectric characterization.

Physical Property Part. The CaOFeS structure exhibits the noncentrosymmetric space group $P6_3mc$, and taking into account the triangular-shaped configuration of two successive $FeOS_3$ layers, some peculiar electronic features are expected. Magnetic susceptibility and resistivity measurements as a function of the temperature were carried out in the range from 5 to 300 K. These measurements have been performed on single-crystal materials. For a platelet-like crystal with the magnetic field applied perpendicularly to the thinnest dimension, i.e., perpendicular to the *c*-axis direction, the magnetic susceptibility curve collected versus T exhibits an antiferromagnetic-like transition, clearly observed around 70 K (Figure 5a), together with a paramagnetic behavior, which can

DOI: 10.1021/acs.inorgchem.5b00879
Inorg. Chem. 2015, 54, 6560−6565

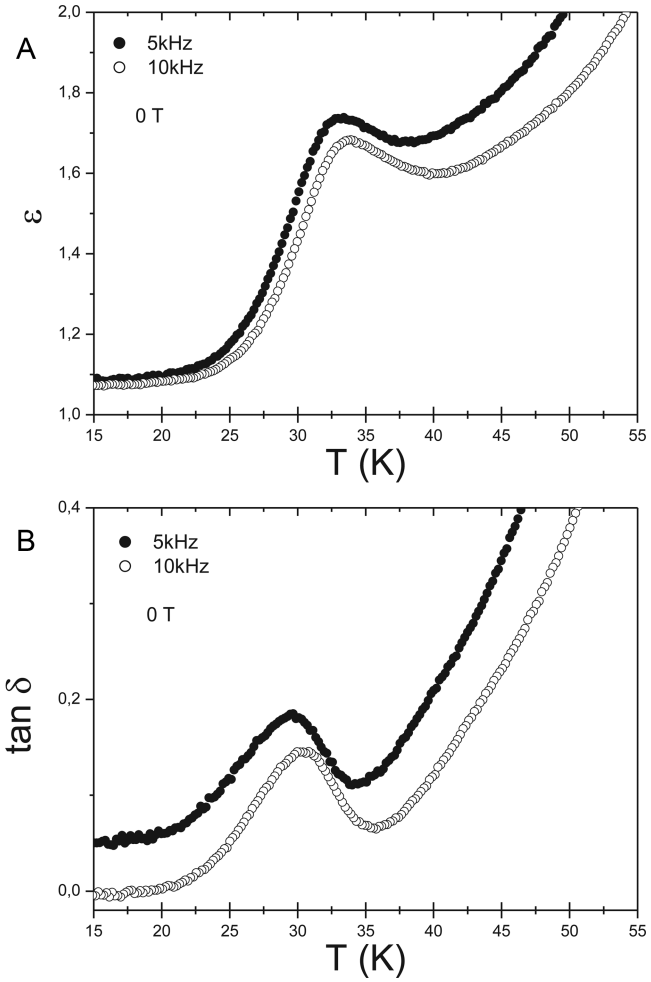

Figure 6. Thermal dependence of the (a) dielectric permittivity ε (f = 5 and 10 kHz) and (b) corresponding dielectric losses tan δ without an applied magnetic field.

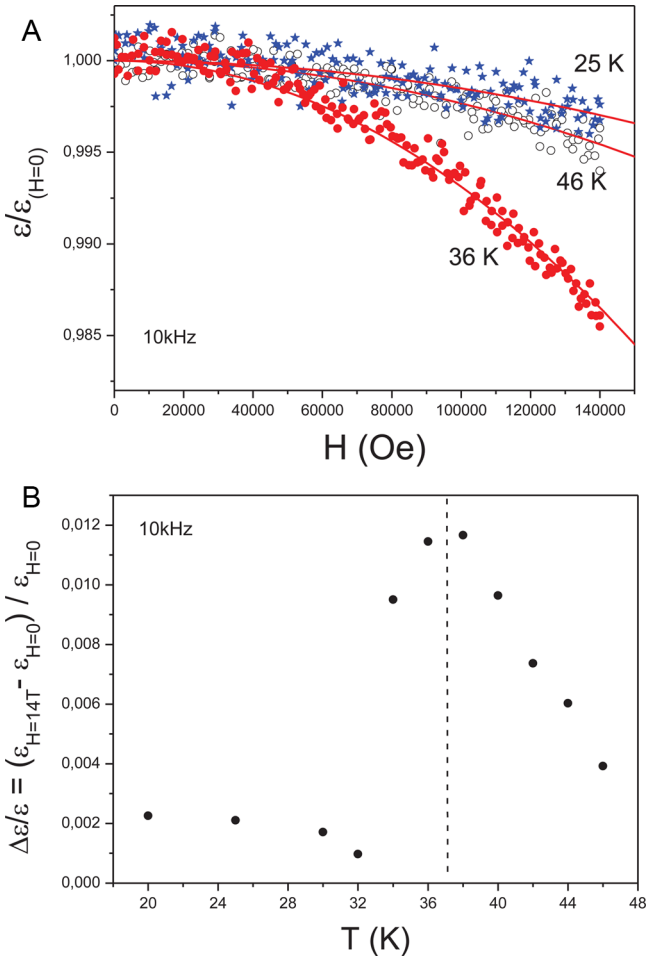

Figure 7. (a) Variation of ε as a function of the magnetic field for some characteristic temperatures. Also shown is the H^2 variation as red plain lines. (b) Relative variation $\Delta\varepsilon/\varepsilon = (\varepsilon_{H=14T} - \varepsilon_{H=0})/\varepsilon_{H=O}$ depending on the temperature.

be viewed beyond 200 K from the $\chi^{-1}(T)$ linearity (inset of Figure 5a), in agreement with the lack of magnetic contribution detected on NPD data collected at room temperature.[5] In addition, the T-dependent resistivity measurements reveal a semiconducting behavior with relatively high ρ values (Figure 5b). Note that, under 80 K, resistance values reach the experimental detection limit of our device (10^6 Ω). Consequently, this work has been completed by T-dependent dielectric constant (ε) and dielectric loss (tan δ) measurements for two selected frequencies (5 and 10 kHz, respectively) without any applied external magnetic field and performed along the c axis. In spite of its relatively high ρ values, the CaOFeS compound remains too conductive so dielectric constant and dielectric loss measurements were limited to the low-temperature range (with tan δ < 0.2, i.e., T < 40 K). A transition in both the dielectric constant and loss is observed at $T \approx 33$ K, and that transition temperature exhibits a weak frequency dependence (Figure 6a,b). This transition in the dielectric constant fits to the peak in the specific heat at 35 K reported in ref 5. Because the latter is connected to the setting of a long-range antiferromagnetic order between 40.6 and 26 K, our observation supports to the existence of a magnetodielectric coupling. In addition, we have measured the variation of the dielectric constant ε as a function of the magnetic field H, as shown in Figure 7a for a geometry such as $H \perp E$. A clear dependence is observed in the temperature range 32−46 K, indicating a magnetocapacitance. This is also evidenced in the negative magnetodielectric effect observed in the $\varepsilon = f(H)$ curves (Figure 7a), which go through a minimum close to T_N (curve collected at 36 K). More quantitatively, this variation is quadratic with the applied field, as was expected for the bilinear component of magnetoelectric coupling. The maximum of the effect is observed at $T \approx 36$ K (Figure 7b). That characteristic temperature can be related to the anomaly observed on $\varepsilon = f(T)$ curves but does not correspond to the magnetic transition at 70 K in our sample. The change in $\varepsilon(T)$ at 36 K is in good agreement with the T_N value reported in ref 5. Clearly, this magneto dielectric effect appears to be related to the magnetic ordering.

CONCLUDING REMARKS

The oxysulfide CaOFeS was isolated as a single crystal, and the actual stoichiometry was jointly validated by NPD diffraction refinements. The structural analyses and physical measurements revealed a hexagonal polar structure with two specific transitions: an antiferromagnetic transition at 70 K and a transition in the dielectric constant around 36 K. According to previous studies,[3−5] this material is very difficult to obtain as a single phase. Compared to the $X(T)$ curve showing a broad transition peak at 120 K in ref 5, our transition at 70 K is most

DOI: 10.1021/acs.inorgchem.5b00879
Inorg. Chem. 2015, 54, 6560−6565

probably coming from an impurity. This point can be correlated to the systematic unidentified surface layer that was detected from the SEM observations on single-crystal material. The impurity identified during the TEM study carried out with the bulk material is related to a new $CaFe_{5/4}O_xS$ structure. So, a phase separation between CaOFeS and this unknown phase, especially at the level of the crystal surface, cannot be excluded even if the single-crystal diffraction data analyses have not evidenced the coexistence of both structures and the HREM observations have not revealed some extended defects. The next step will be to isolate this new phase in order to solve its structure and determine its physical properties.

■ ASSOCIATED CONTENT

Supporting Information

X-ray crystallographic data for CaOFeS in CIF format and NPD data at room temperature. The Supporting Information is available free of charge on the ACS Publications website at DOI: 10.1021/acs.inorgchem.5b00879.

■ AUTHOR INFORMATION

Corresponding Author

*E-mail: denis.pelloquin@ensicaen.fr.

Notes

The authors declare no competing financial interest.

■ ACKNOWLEDGMENTS

The authors acknowledge financial support from the French Agence Nationale de la Recherche (ANR), through the program "Investissements d'Avenir" (ANR-10-LABX-09-01), LabEx EMC^3. The authors are grateful to F. Veillon for the dielectric measurements, Dr. S. Gascoin for SEM observations, and X. Larose for technical support in TEM.

■ REFERENCES

(1) Clarke, S. J.; Adamson, P.; Herkelrath, S. J. C.; Rutt, O. J.; Parker, D. R.; Pitcher, M. J.; Smura, C. F. *Inorg. Chem.* **2008**, *47*, 8473−8486.
(2) Johrendt, D.; Hosono, H.; Hoffmann, R. D.; Pöttgen, R. *Z. Kristallogr.* **2011**, *226*, 435−446.
(3) Jha, A.; Igiehon U. O.; Grieveson, P. *Scand. J. Metall.* **1991**, *20*.
(4) Selivanov, E. N.; Chumarev, V. M.; Gulyaeva, R. I.; Marevich, V. P.; Vershinin, A. D.; Pankratov, A. A.; Korepanova, E. S. *Inorg. Mater.* **2004**, *40*, 969−974.
(5) Jin, S. F.; Huang, Q.; Lin, Z. P.; Li, Z. L.; Wu, X. Z.; Ying, T. P.; Wang, G.; Chen, X. L. *Phys. Rev. B* **2015**, *91*, 094420.
(6) Sambrook, T.; Smura, C. F.; Clarke, S. J. *Inorg. Chem.* **2007**, *46*, 2571−2574.
(7) Petrova, S. A.; Marevich, V. P.; Zakharov, R. G.; Selivanov, E. N.; Chumarev, V. M.; Udoeva, L. Yu. *Dokl. Chem.* **2003**, *393*, 255−258.
(8) Sheldrick, G. M. *SADABS Program for Empirical Absorption Correction of Area Detector Data*; University of Göttingen: Göttingen, Germany, 1996.
(9) Oszlanyi, G.; Suto, A. *Acta Crystallogr.* **2008**, *A64*, 123−134.
(10) Palatinus, L.; Chapuis, G. *J. Appl. Crystallogr.* **2007**, *40*, 786−790.
(11) Palatinus, L.; Van der Lee, A. *J. Appl. Crystallogr.* **2008**, *41*, 975−984.
(12) Petricek, V.; Dusek, M.; Palatinus, L. *Jana2006 Structure Determination Software Programs*; Institute of Physics: Praha, Czech Republic, 2006.
(13) Flack, H. D. *Acta Crystallogr.* **1983**, *A39*, 876−881.

DOI: 10.1021/acs.inorgchem.5b00879
Inorg. Chem. 2015, 54, 6560−6565